*cells*

MDPI

*Article*

# Toxicoproteomic Profiling of *hPXR* Transgenic Mice Treated with Rifampicin and Isoniazid

Christopher Trent Brewer [1,2,3,†] , Kiran Kodali [4,†], Jing Wu [1], Timothy I. Shaw [4,5], Junmin Peng [4,6,7,*] and Taosheng Chen [1,*]

[1] Department of Chemical Biology and Therapeutics, St. Jude Children's Research Hospital, Memphis, TN 38105, USA; cbrewe16@uthsc.edu (C.T.B.); jing.wu@stjude.org (J.W.)
[2] College of Medicine, University of Tennessee Health Science Center, Memphis, TN 38163, USA
[3] Integrated Biomedical Sciences Program, College of Graduate Health Sciences, University of Tennessee Health Science Center, Memphis, TN 38163, USA
[4] Center for Proteomics and Metabolomics, St. Jude Children's Research Hospital, Memphis, TN 38105, USA; kiran.kodali@stjude.org (K.K.); tim.shaw@stjude.org (T.I.S.)
[5] Department of Computational Biology, St. Jude Children's Research Hospital, Memphis, TN 38105, USA
[6] Department of Structural Biology, St. Jude Children's Research Hospital, Memphis, TN 38105, USA
[7] Department of Developmental Neurobiology, St. Jude Children's Research Hospital, Memphis, TN 38105, USA
* Correspondence: junmin.peng@stjude.org (J.P.); taosheng.chen@stjude.org (T.C.); Tel.:+901-595-7499 (J.P.); +901-595-5937 (T.C.)
† These authors contributed equally to this work.

check for updates

**Abstract:** Tuberculosis is a global health threat that affects millions of people every year, and treatment-limiting toxicity remains a considerable source of treatment failure. Recent reports have characterized the nature of *hPXR*-mediated hepatotoxicity and the systemic toxicity of antitubercular drugs. The antitubercular drug isoniazid plays a role in such pathologic states as acute intermittent porphyria, anemia, hepatotoxicity, hypercoagulable states (deep vein thrombosis, pulmonary embolism, or ischemic stroke), pellagra (vitamin $B_3$ deficiency), peripheral neuropathy, and vitamin $B_6$ deficiency. However, the mechanisms by which isoniazid administration leads to these states are unclear. To elucidate the mechanism of rifampicin- and isoniazid-induced liver and systemic injury, we performed tandem mass tag mass spectrometry-based proteomic screening of $mPxr^{-/-}$ and *hPXR* mice treated with combinations of rifampicin and isoniazid. Proteomic profiling analysis suggested that the *hPXR* liver proteome is affected by antitubercular therapy to disrupt [Fe–S] cluster assembly machinery, [2Fe–2S] cluster-containing proteins, cytochrome P450 enzymes, heme biosynthesis, homocysteine catabolism, oxidative stress responses, vitamin $B_3$ metabolism, and vitamin $B_6$ metabolism. These novel findings provide insight into the etiology of some of these processes and potential targets for subsequent investigations. Data are available via ProteomeXchange with identifier PXD019505.

**Keywords:** anemia; antitubercular therapy; cytochrome P450; drug-induced liver injury; heme biosynthesis; hypercoagulability; iron–sulfur cluster; pellagra; vitamin $B_3$; vitamin $B_6$

## 1. Introduction

Tuberculosis (TB) is a leading cause of death from infectious diseases worldwide, second only to human immunodeficiency virus [1]. The treatment for latent TB infections comprises isoniazid treatment for 6 months. Treatment for active TB infections comprises 4 months of rifampicin, isoniazid, pyrazinamide, and ethambutol. Hepatotoxicity decreases adherence to antitubercular treatment

regimens and contributes to treatment failure, disease relapse, and drug resistance [2]. Hepatotoxicity is a leading cause of TB therapy treatment failure, with up to 28% of all anti-TB treatment failure attributed to toxicity [3,4]. Antitubercular therapy may also be associated with acute intermittent porphyria [5,6], sideroblastic anemia [7–10], hypercoagulability [11–13], peripheral neuropathy [14–16], porphyria cutanea tarda [17], vitamin $B_3$ deficiency [18–20], and vitamin $B_6$ deficiency [8,14,21,22].

Further characterization of the mechanism of antitubercular liver and systemic injury is necessary to update clinical guidance to prevent or ameliorate injury. The human pregnane X receptor (hPXR) is implicated in the hepatotoxicity of pharmaceuticals [23,24] and herbal supplements [25]. This hepatotoxicity is associated with increased protoporphyrin IX (PPIX), which is a precursor to heme suitable for quantification via high-throughput fluorescence imaging [26]. The iron-dependent modulation of ferrochelatase (FECH) and aminolevulinic acid synthase 1 (ALAS1) is also driven by metabolites of isoniazid [27]. Rifampicin is a well-known inducer of drug-metabolizing enzymes and transporters via hPXR. The hPXR is a nuclear hormone receptor that responds to endobiotics and xenobiotics by increasing transcription of the genes involved in the elimination of toxic compounds, such as cytochrome P450 (CYP) enzymes, glucuronosyltransferases, sulfotransferases, ATP-binding cassette transports, and others. Isoniazid is a vitamin $B_6$ antimetabolite that is associated with clinical syndromes exacerbated by and associated with vitamin $B_6$ depletion.

Isoniazid and rifampicin treatment alone and in combination can lead to drug toxicity. The toxicity of the combination may be more severe and/or frequent than either drug alone. In mice, isoniazid- and rifampicin-induced hepatotoxicity is hPXR-dependent and associated with accumulation of PPIX. These antitubercular drugs are administered orally and undergo first-pass metabolism in the liver. Consequently, many of the processes involved in the pathophysiology of systemic antitubercular toxicity are located in the liver.

We investigated the effects of the antitubercular drugs rifampicin and isoniazid by tandem mass tag (TMT) mass spectrometry-based proteomic screening of the livers from mice with *Pxr* knockout ($mPxr^{-/-}$) and the $mPxr^{-/-}$ mice with transgenic *hPXR* (*hPXR* mice) treated with rifampicin, isoniazid, or a combination of rifampicin and isoniazid. We specifically used *hPXR* transgenic mice because rifampicin is a specific agonist for hPXR and not mouse pregnane X receptor (PXR) [28]. Proteomic profiling identified changes in [Fe–S] cluster assembly machinery proteins, [Fe–S] cluster-containing proteins, CYP and steroid metabolism enzymes, heme synthesis and degradation, iron metabolism, nuclear hormone receptors, oxidative stress, tryptophan metabolism, vitamin $B_3$ metabolism, vitamin $B_6$ metabolism, and wound-healing and inflammation pathways. This study is the first to investigate the role of hPXR in these pathways by using both rifampicin and isoniazid in *hPXR* mice (compared to $mPxr^{-/-}$ mice) to identify hPXR-mediated changes in protein levels.

## 2. Materials and Methods

### 2.1. Reagents

We obtained dimethyl sulfoxide from Corning (Corning, NY, USA), Dulbecco phosphate-buffered saline (PBS) from Gibco (Little Rock, AR, USA), and rifampicin and isoniazid from Sigma-Aldrich (St. Louis, MO, USA). MS-related reagents included LC-MS grade acetonitrile, water, ammonium acetate, ammonium hydroxide, and formic acid from Sigma-Aldrich (St. Louis, MO, USA).

### 2.2. Antibodies

We purchased primary antibodies from the following sources: anti-FECH mouse monoclonal antibody (sc-377377) from Santa Cruz Biotechnology (Dallas, TX, USA; diluted 1:5000), anti-ALAS1 mouse monoclonal antibody (ab54758) from Abcam (Cambridge, UK; diluted 1:2000), and anti-CYP3A4 K03 mouse monoclonal antibody at a dilution of 1:1000 [29–31]. We purchased goat anti-mouse infrared dye (IRDye)-conjugated (680 RD and 800 CW) secondary antibodies from LI-COR (Cambridge, UK) and used them at a dilution of 1:10,000 to visualize proteins [27].

### 2.3. Mice

We used 8-to-12-week-old *hPXR* transgenic and *mPxr*$^{-/-}$ C57BL/6 mice for all in vivo experiments [28]. The mice were provided with food (Purina; St. Louis, MO, USA) containing rifampicin (300 mg/kg in chow) and autoclaved water containing isoniazid (1.2 g/L in water) ad libitum for 6 months (Figure 1A). We collected sera weekly to monitor liver function. All animal studies were approved by the Institutional Animal Care and Use Committee at St. Jude Children's Research Hospital (St. Jude), and mice were housed in Association for Assessment and Accreditation of Laboratory Animal Care-accredited facilities. Quantification of liver function tests from plasma and sera was performed on the ABX Pentra instrument from Medline Industries (Northfield, IL, USA). HORIBA Enzyme Assays from Fisher Scientific (Waltham, MA, USA) were used to analyze alkaline phosphatase (ALP) (Catalogue # 23600417), alanine aminotransferate (ALT) (Catalogue # 23600418), direct bilirubin (Catalogue # 23600426), and total bilirubin (Catalogue # 23600430). Liver damage was evaluated by hematoxylin and eosin staining, and pathologic scoring was performed by board-certified pathologists.
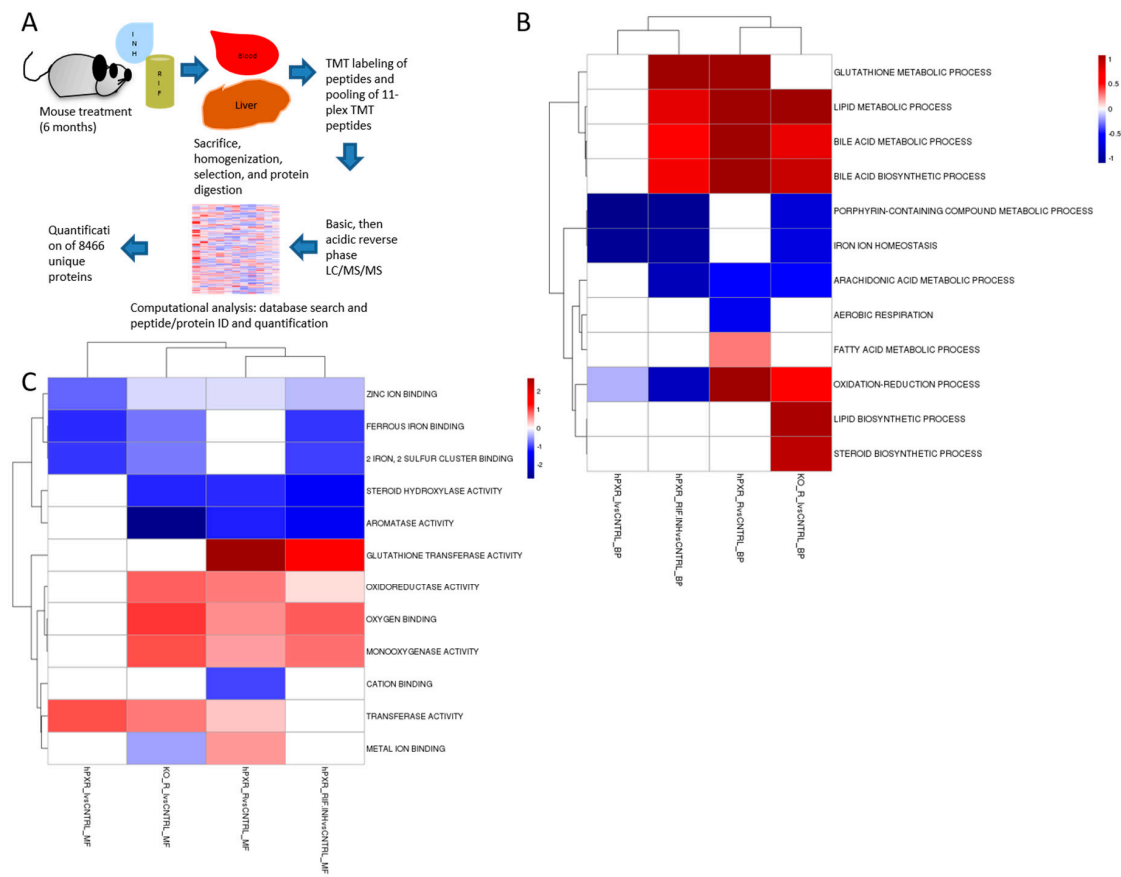
**Figure 1.** Experimental scheme and gene ontology enrichment analysis. (**A**) Schematic diagram of proteomic analysis workflow: *hPXR* transgenic or *mPxr*$^{-/-}$ mice were treated with rifampicin (RIF, 300 mg/kg chow), isoniazid (INH, 1.2 g/L water), or both. Liver tissues were lysed, digested into peptides, and labeled with tandem mass tags (TMTs). The labeled samples were equally mixed and further fractionated by basic pH reverse-phase liquid chromatography (LC). The fractions were collected and further analyzed by acidic pH reverse-phase LC-MS/MS. During ion fragmentation, the TMT regents were cleaved to produce reporter ions for quantification. The collected data were searched against a database to identify peptides. Although the peptides were identified by MS/MS, quantification was achieved by the fragmented reporter ions in the same MS/MS scans. Then, the peptide quantification data were corrected for mixing errors, summarized to derive protein quantification, and subjected to statistical analysis to determine cutoffs for altered proteins and evaluate the associated false discovery rate. (**B,C**) Clustering analysis of the up-regulated and down-regulated proteins in *hPXR* mice treated with rifampicin and/or isoniazid, as compared to control *hPXR* mice, and in *mPxr*$^{-/-}$ mice treated with rifampicin and isoniazid. Differential protein expression was performed using a moderated T-test implemented in linear models for microarray (LIMMA). LIMMA was used to perform differential gene expression analysis. A cutoff *p*-value of 0.05 was used as the differential cutoff. Fishers-exact test using the up-regulated and down-regulated genes were tested against GO-Biological Process (BP) (**B**) and GO-Molecular Function (MF) (**C**) gene sets. An enrichment score was calculated based on the -log20(p-value). Log20 was chosen to normalize 0.05 to a score of 1.0 as a reference. Red indicates up-regulated proteins and blue indicates down-regulated proteins. hPXR_IvsCNTRL = Isoniazid-treated *hPXR* mice compared to control *hPXR* mice; hPXR_RIF.INHvsCNTRL = Rifampicin and isoniazid-treated *hPXR* mice compared to control *hPXR* mice; hPXR_RvsCNTRL = Rifampicin-treated *hPXR* mice compared to control *hPXR* mice; KO_R_IvsCNTRL = Rifampicin and isoniazid-treated *mPxr*$^{-/-}$ mice compared to rifampicin and isoniazid treated *hPXR* mice.

## 2.4. Immunoblot Analysis

Livers were collected, flash frozen, and lysed [50 mM 4-(2-hydroxyethyl)-1-piperazineethanesulfonic acid (HEPES), pH 8.5, 8 M urea, and 0.5% sodium deoxycholate], and 100 μg of protein was digested with LysC from Wako Chemicals (Richmond, VA, USA) in the presence of 1,4-dithiothreitol at an enzyme-to-substrate ratio of 1:100 for 2 h as described previously [32]. Then, the samples were diluted to a final concentration of 2 M urea with 50 mM HEPES, pH 8.5, and stored at −80°C until immunoblot analysis was performed. NuPAGE LDS loading buffer and reducing agent from Invitrogen (Carlsbad, CA, USA) were used to prepare protein lysates for electrophoresis. Protein were separated with NuPAGE 4%–12% Bis-Tris protein gels (Invitrogen, Carlsbad, CA, USA), and protein sizes were estimated by using the Kaleidoscope protein marker from Bio-Rad (Hercules, CA, USA). Proteins were transferred from gels to iBlot nitrocellulose membranes (Invitrogen) by dry transfer. Membranes were incubated for 1 h at room temperature (RT) in tris buffered saline with tween (TBST) blocking buffer (LI-COR, Lincoln, NE, USA) before probing with primary antibodies. Membranes were incubated with primary antibodies overnight at 4°C and then incubated with secondary antibodies for 1 h at RT before visualization. Then, we stripped the membranes with NewBlot Nitro stripping buffer (LI-COR), incubated them with an anti–β-actin primary antibody (a5441; Sigma-Aldrich, St. Louis, MO, USA; diluted 1:1000) overnight at 4°C, and then incubated them with a secondary antibody for 1 h at RT. We visualized the protein bands with an Odyssey infrared imager (LI-COR Biosciences) and determined the relative intensity of each band by normalizing their intensities to that of the actin band [27,33].

## 2.5. Proteomic Profiling

Mouse livers were prepared as described for immunoblotting, and the profiling was performed following the optimized procedure [34]. To generate peptides for liquid chromatography (LC) and mass spectrometry (MS) analyses, the protein samples were digested with trypsin from Promega (Madison, WI, USA) after resuspension in 50 mM HEPES at an enzyme-to-substrate ratio of 1:50 for

3 h. The resulting peptides were reduced by adding 1 mM 1,4 –dithiothreitol for 30 min at RT and were alkylated with 10 mM iodoacetamide for 30 min at RT in the dark. The reaction was quenched by adding trifluoroacetic acid. This acidified peptide mixture was desalted by C18 cartridges from Harvard Apparatus (Holliston, MA, USA). The desalted eluates were dried and resuspended in 50 mM HEPES, pH 8.5.

Samples were labeled with 11-plex TMTs from Thermo Fisher (Waltham, MA, USA), according to the manufacturer recommendations. After labeling, the samples were combined, desalted, and fractionated with an off-line basic pH reverse phase C18 LC using high-performance liquid chromatography (HPLC; Agilent 1220) from Agilent Technologies (Santa Clara, CA, USA). The collected concatenated fractions were dried, resuspended in 5% formic acid, and analyzed by acidic pH reverse-phase LC-MS/MS. The samples were fractionated with a nanoscale capillary reverse-phase C18 column on a nanoAcquity HPLC from the Waters Corporation (Millford, MA, USA). The eluents were ionized by electrospray ionization and detected with an inline Orbitrap Fusion MS instrument from Thermo Fisher (Richmond, VA, USA). MS was performed in a data-dependent mode, with a survey scan (60,000 resolution, $1 \times 10^6$ automatic gain control target and 50-microsecond maximal ion time) and 20 MS/MS high resolution scans (60,000 resolution, $1 \times 10^5$ automatic gain control target and 150 microsecond maximal ion time, 38 high-energy collision-induced dissociation normalized energy, 1 m/z isolation window, and 20-s dynamic exclusion).

Raw mass spectra were processed by the JUMP program [35]. The resultant data were compared to the UniProt mouse database and concatenated with a reversed protein sequence decoy database. Searches were performed with a mass tolerance of 25 ppm for precursor ions and 15 ppm mass tolerance for fragment ions, fully tryptic restriction with two maximum missed cleavages, three maximum modification sites, and assignment of the *a*, *b*, and *y* ions. TMT tags on lysine residues and N-termini (+229.162932 Da) and the carbamidomethylation of cysteine residues (+57.021 Da) were used for determining static modifications, and methionine oxidation (+15.99492 Da) was considered a dynamic modification. Mass spectra were filtered by mass accuracy and matching scores to reduce the false discovery rate (FDR) to approximately 1%. The proteins were quantified by summarizing reporter ion counts across all matched peptide spectrums with the JUMP software suite [36]. Clustering analysis was performed with R v.3.0.1.

## 2.6. Statistical Analysis

We pooled data from three independent experiments and performed statistical analyses with GraphPad Prism 7.0 software. Venn diagrams were generated by using the Venny software v.2.0.2. All parametric data were expressed as the mean and standard error. To compare group means for qRT-PCR analysis, we used a two-way analysis of variance (ANOVA) and Tukey post hoc analysis. For immunoblot analysis, we used a one-way ANOVA and Dunnett post hoc analysis. We determined the changed proteins using the following steps based on previous published cutoffs with slight modifications [37]. (1) We applied a commonly used cutoff of *p* value (0.05) based on one-way ANOVA. (2) We used an additional cutoff the magnitude of change (*z* score > 2). The *z* score was defined by evaluating standard deviation of the experiments through analyzing biological replicates (null experiments) and then applying the standard deviation for *z* score conversion [36]. The *z* score of 2 was usually equivalent to > 1.15-relative change for up-regulated proteins and < 0.85-relative change for down-regulated proteins unless otherwise noted. (3) We performed permutation analysis (n = 1000 permutations) and found that the FDR was below 20%. The mass spectrometry proteomics data have been deposited to the ProteomeXchange Consortium via the PRIDE [38] partner repository with the dataset identifier PXD019505.

## 3. Results

### 3.1. Hepatopathic Changes

We observed hepatotoxic changes in *mPxr⁻/⁻* and *hPXR* transgenic C57BL/6 mice treated for 6 months with combinations of 300 mg/kg rifampicin in chow and 1.2 g/L isoniazid in water (Figure 1A). This was evidenced by markedly increased direct bilirubin (Figure 2C) and alkaline phosphatase (ALP; Figure 2A) in *hPXR* mice treated with both rifampicin and isoniazid. We identified protein changes specific to mouse strain and drug treatment (Supplemental Figure S1). Rifampicin increased CYP3A protein levels in an *hPXR*-dependent manner (Supplementary Figure S2, S3, and S4C), and isoniazid decreased FECH protein levels (Supplementary Figures S2, S3, and S4A) and increased ALAS1 (Supplementary Figures S2, S3, and S4B). Histologic examination revealed the presence of bile plugs (Figure 3C) and higher hepathopathologic (HP) scores (Figure 3A) in *hPXR* mice treated with both rifampicin and isoniazid. These changes are consistent with previous reports of *hPXR*-dependent hepatotoxicity in mice treated with isoniazid and rifampicin [27,39,40].
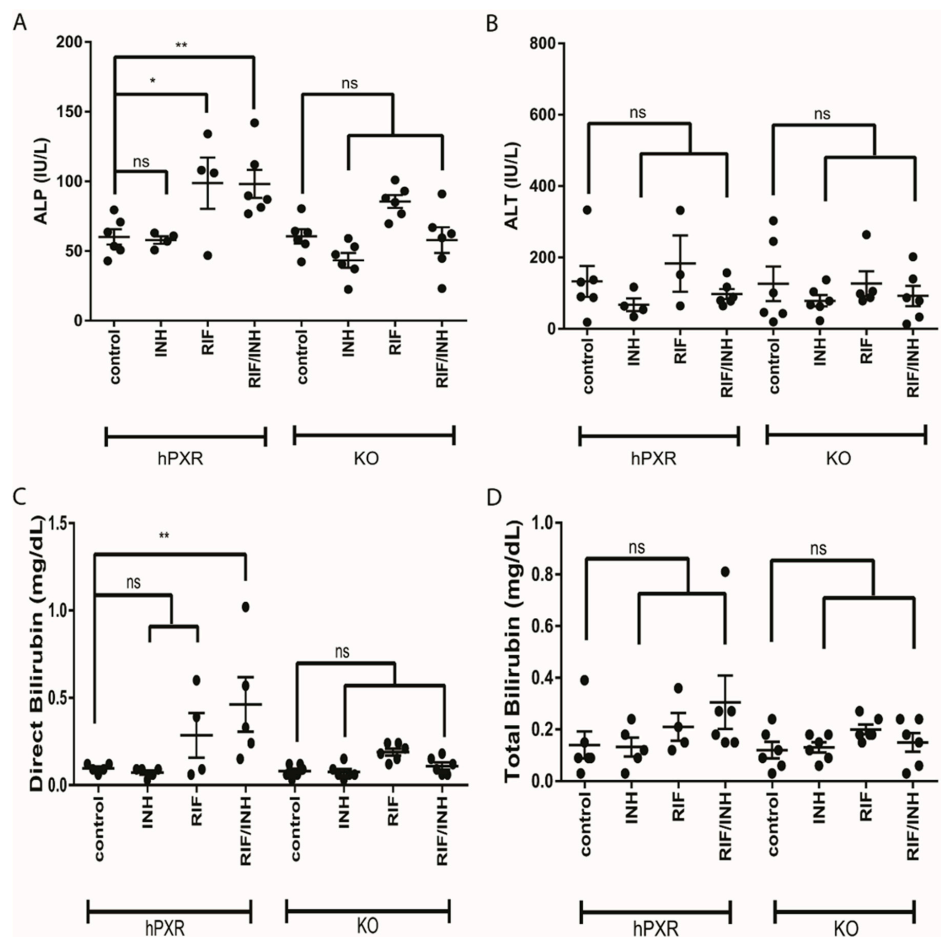


**Figure 2.** Liver function tests from human pregnane X receptor (*hPXR*) and *mPxr⁻/⁻* knockout (KO) mice treated with rifampicin (RIF) and isoniazid (INH). Sera were analyzed for markers of hepatotoxicity before liver collection. (**A**) Alkaline phosphatase (ALP), (**B**) alanine aminotransferate (ALT), (**C**) direct bilirubin, and (**D**) total bilirubin are shown. Data are expressed as the mean ± SEM. One-way ANOVA followed by Dunnett post hoc analysis was used to compare group means. ** $p < 0.01$, * $p < 0.05$, and ns (not significant).
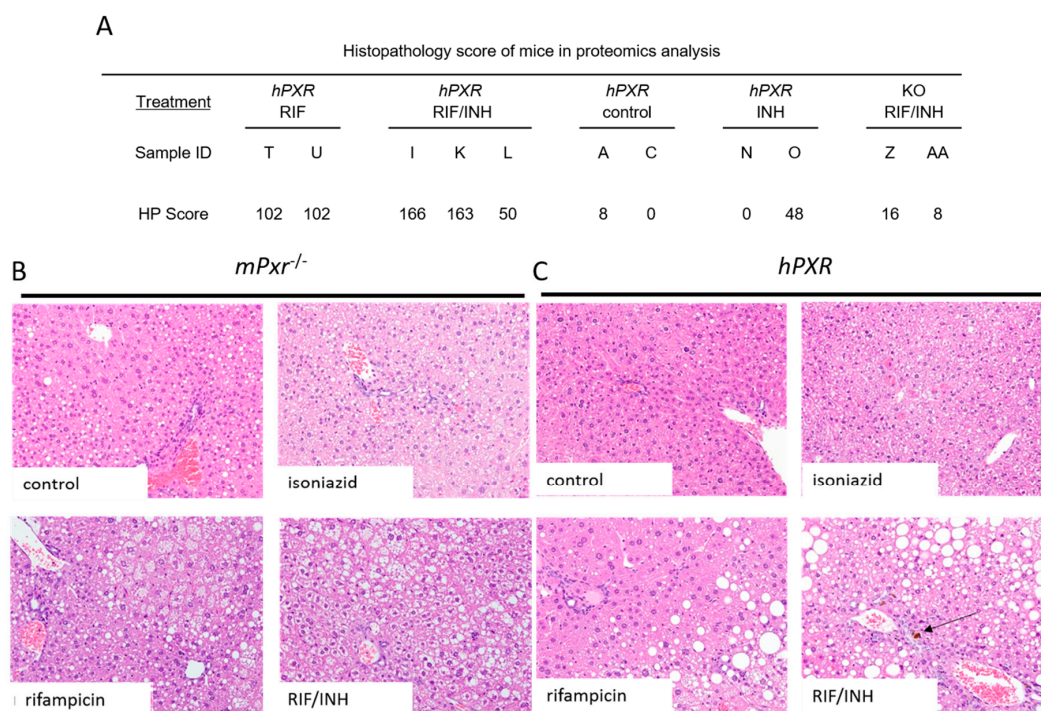
A

Histopathology score of mice in proteomics analysis

| Treatment | *hPXR* RIF | | *hPXR* RIF/INH | | | *hPXR* control | | *hPXR* INH | | KO RIF/INH | |
|---|---|---|---|---|---|---|---|---|---|---|---|
| Sample ID | T | U | I | K | L | A | C | N | O | Z | AA |
| HP Score | 102 | 102 | 166 | 163 | 50 | 8 | 0 | 0 | 48 | 16 | 8 |



**Figure 3.** Histopathology of mouse livers. Semiquantitative histopathology scoring was performed by a board-certified veterinary pathologist. (**A**) Total hepatopathology scores (HP) were determined by scoring inflammation, karyomegaly, steatosis, bile pigment, and necrosis. Hematoxylin and eosin staining of *hPXR* (**B**) and *mPxr*$^{-/-}$ (**C**) mouse livers (20×), arrows indicate bile plugs.

## 3.2. Quantitative Analysis of the Liver Proteome

We identified and quantified 8466 proteins in the livers of *mPxr*$^{-/-}$ and *hPXR* mice (Figure 1A). Clustering analysis revealed similar protein changes within groups (Figure 1B,C, and Supplementary Figures S5 and S6). The protein changes observed in *hPXR* mice treated with the drug combination and not in the *mPxr*$^{-/-}$ mice are most likely *hPXR*-specific. The proteins that were changed in both strains most likely represent *hPXR*-independent effects. Supplementary Figure S1 summarizes these protein changes in the different mouse strains (*hPXR* or *mPxr–/–* mice) and drug treatment groups (also see Supplementary Figure S6; Supplementary Tables S12, S13, and S14). Therefore, distinct protein changes occurred between the treatment groups, which we further analyzed to identify the proteins that mediate hPXR-induced isoniazid and rifampicin toxicity.

### 3.2.1. Heme Biosynthesis and Degradation

Heme biosynthesis disruption is reported to occur after rifampicin and isoniazid treatment in mice and is associated with increased liver levels of PPIX [40]. ALAS1 increased at a 1.9-relative change in *hPXR* mice treated with both rifampicin and isoniazid, a 2.6-relative change in *hPXR* mice treated with isoniazid alone, and a 1.4-relative change in *mPxr*$^{-/-}$ mice treated with the rifampicin and isoniazid combination. However, these changes did not significantly differ across the groups (Supplementary Table S1; $p = 0.28$). FECH decreased ($p < 0.0001$) in all groups, with a greater decrease (0.39-relative change to 0.5-relative change) in mice treated with isoniazid alone or in combination with rifampicin.

We found other heme biosynthesis proteins that changed with antitubercular therapy (Supplementary Table S1). These changes can be associated with an accumulation of toxic compounds related to heme biosynthesis, such as PPIX and others. Uroporphyrinogen-III synthase (UROS) significantly ($p = 0.012$) increased at a 1.19-relative change in *hPXR* mice treated with both rifampicin and isoniazid and a 1.31-relative change in *hPXR* mice treated with rifampicin. UROS also increased at a 1.38-relative change in *mPxr*$^{-/-}$ mice treated with both rifampicin and isoniazid. These data suggest

that UROS is increased by rifampicin in an *hPXR*-independent manner. Protoporphyrinogen oxidase (PPOX) significantly decreased ($p = 0.013$) with all treatments in an *hPXR*-independent manner by 0.69- to 0.85-relative change, and this effect was more pronounced in *hPXR* mice treated with both rifampicin and isoniazid (0.69-relative change) than in *mPxr$^{-/-}$* mice (0.83-relative change). Biliverdin reductase (BLVRA) significantly decreased (0.82- to 0.92-relative change) in all treatment groups, independent of *hPXR* status ($p = 0.032$). These data are consistent with previous reports of ALAS1 up-regulation and FECH down-regulation due to isoniazid and its metabolites and demonstrate a potential for the accumulation of toxic heme metabolites [27,39,40].

Ferritin light chain (FTL1) significantly decreased ($p = 8.42 \times 10^{-5}$) in all treatment groups (Supplementary Table S3). FTL1 was most severely decreased in *hPXR* mice treated with both rifampicin and isoniazid (0.28-relative change), followed by *hPXR* mice treated with isoniazid alone (0.36-relative change). ABCB7 significantly decreased (0.83-relative change) in *hPXR* mice treated with rifampicin and isoniazid ($p = 0.019$) (Supplementary Table S3). ABCB7 also decreased in *hPXR* mice treated with rifampicin (0.79-relative change) and modestly decreased in *mPxr$^{-/-}$* mice treated with both rifampicin and isoniazid (0.91-relative change). These data are consistent with reports of anemia in patients with tuberculosis who are treated with antitubercular drugs [7,8,10].

### 3.2.2. CYP Induction

CYP2B10 is the most up-regulated CYP and significantly increased ($p = 0.0003$) with rifampicin treatment alone (2.49-relative change) and with the rifampicin and isoniazid combination treatment (4.95-relative change) in *hPXR* mice (Supplementary Table S4). CYP3A11—the mouse CYP3A4 ortholog [41]—significantly increased ($p = 0.0008$) in *hPXR* mice treated with rifampicin (4.64-relative change) and treated with both rifampicin and isoniazid (3.89-relative change). Several CYPs decreased with isoniazid treatment: CYP1A2 (0.48-relative change), CYP2A12 (0.78-relative change), CYP2A5 (0.62-relative change), and CYP2D26 (0.71-relative change). CYP2E1 significantly increased ($p = 0.00035$) in *hPXR* mice treated with the rifampicin and isoniazid combination (1.22-relative change) or isoniazid alone (1.18-relative change). CYP2E1 also increased in *mPxr$^{-/-}$* mice treated with both rifampicin and isoniazid (1.47-relative change). Polymorphisms associated with increased CYP2E1 activity in humans increase the incidence of drug-induced liver injury (DILI) [42–44]. Inhibiting CYP2E1 is protective against isoniazid-induced hepatotoxicity in mice [45]. CYP2E1 wild-type mice are more susceptible to DILI than are mice lacking the gene [46]. Therefore, CYP2E1 upregulation by rifampicin in an *hPXR*-independent manner may contribute to DILI.

The nuclear receptors HNF1A, NR3C, and NR5A significantly decreased in *hPXR* mice (Supplementary Table S2), but other nuclear receptors were not significantly changed, suggesting that the changes observed in target genes (i.e., CYP enzymes) were caused by the activation of these nuclear receptors rather than a change in the expression of the receptors.

### 3.2.3. Oxidative Stress, Wound Healing, and Inflammation

Many isoforms of glutathione S transferase mu (GSTM), which detoxify electrophilic compounds and cluster on chromosome 1p13.3, significantly changed in *hPXR* mice (Supplementary Table S5; $p < 0.0001$). GSTM-1, -2, -3, -4, -5, -6, and -7 increased relative to the change in *hPXR* (1.59- to 3-relative change) and *mPxr$^{-/-}$* (1.16- to 1.61-relative change) mice treated with the rifampicin and isoniazid combination, decreased (0.79- to 0.87-relative change) in *hPXR* mice treated with isoniazid alone, and increased with the highest magnitude in *hPXR* mice treated with rifampicin alone (1.55-relative change to 4.5-relative change). GSTM-1 is protective in humans treated with antitubercular drugs, and null alleles are associated with a higher incidence of hepatotoxicity [2,47,48]. Catalase (CAT) also significantly increased ($p = 0.038$) in *hPXR* mice treated with both rifampicin and isoniazid (1.16-relative change) or rifampicin alone (1.45-relative change). NAD(P)H dehydrogenase quinone 1 (NQO1) significantly increased ($p < 0.001$) in *hPXR* mice treated with the rifampicin and isoniazid combination (1.52-relative change) or rifampicin alone (2.6-relative change). In *mPxr$^{-/-}$* mice treated with both

rifampicin and isoniazid, NQO1 increased at a 1.92-relative change. In contrast, NQO1 decreased in *hPXR* mice treated with isoniazid alone (0.87-relative change). The decreased expression of GSTM isoforms may potentiate the hepatotoxicity of antitubercular therapy, whereas the increase in catalase and NQO1 may be protective [49].

Several proteins involved in wound healing and inflammation were affected by antitubercular treatment in our analysis. Protein–glutamine gamma-glutamyltransferase 2 (TGM2) significantly increased (Supplementary Table S6; $p = 0.0058$) in *hPXR* mice treated with both rifampicin and isoniazid (1.12-relative change) or rifampicin alone (1.19-relative change). In contrast, TGM2 was down-regulated in *hPXR* mice treated with isoniazid alone (0.81-relative change) and in $mPxr^{-/-}$ mice treated with the rifampicin and isoniazid combination (0.88-relative change). Collagen alpha-1(IV) (COL4A1) and collagen alpha-1 (VI) (COL6A1) significantly increased ($p < 0.01$) in *hPXR* mice treated with both rifampicin and isoniazid (1.27- and 1.10-relative change, respectively). Annexin A5 (ANXA5) significantly increased ($p = 0.032$) at a 1.56-relative change in *hPXR* mice treated either with the rifampicin and isoniazid combination or rifampicin alone. ANXA5 also increased in $mPxr^{-/-}$ mice treated with both rifampicin and isoniazid (1.22-relative change). The up-regulation of these proteins suggests that tissue injury was induced by the antitubercular drugs [50–52].

### 3.2.4. [Fe–S] Cluster-Containing Proteins

Many [2Fe–2S] cluster-containing proteins are decreased by isoniazid, but we did not observe a significant global down-regulation of [Fe–S] cluster-containing proteins in response to isoniazid (Supplementary Table S7). NADH dehydrogenase ubiquinone iron–sulfur protein 8 (NDUFS8) significantly decreased ($p = 0.0012$) in all treatment groups, but with a lower magnitude of decrease in mice treated with isoniazid alone. Aldehyde oxidase 1 (AOX1) significantly decreased ($p = 0.0023$) with isoniazid alone (0.82-relative change), and xanthine dehydrogenase (XDH) significantly decreased ($p = 0.0079$) at a 0.70-relative change in all *hPXR* groups. The succinate dehydrogenase ubiquinone iron–sulfur subunit (SDHB) significantly decreased ($p = 0.036$) in *hPXR* mice treated with the rifampicin and isoniazid combination (0.86-relative change), but to a lesser extent in the other groups. These changes in SDHB may be *hPXR*-mediated by rifampicin and further decreased by isoniazid administration. NADH dehydrogenase ubiquinone iron–sulfur protein 7 (NDUFS7) significantly increased ($p = 0.012$) in *hPXR* mice treated with isoniazid alone (1.14-relative change) and in $mPxr^{-/-}$ mice treated with both rifampicin and isoniazid (1.20-relative change). NADH dehydrogenase ubiquinone iron–sulfur protein 4 (NDUFS4) significantly increased ($p = 0.033$) in all groups except in *hPXR* mice treated with the rifampicin and isoniazid combination. Iron-responsive element-binding protein 2 (IREB2) significantly increased ($p = 0.039$) in all treatment groups at a 1.18- to 1.42-relative change. Ferrodoxin 1 (FDX1) (Supplementary Table S8) and FECH (Supplementary Table S1) significantly decreased with isoniazid treatment.

Isoniazid may affect a subset of [Fe–S] cluster-containing proteins rather than globally affecting these proteins. The NADH dehydrogenase ubiquinone, also termed complex 1, is composed of multiple subunits and contains eight [Fe–S] clusters: multiples of [2Fe–2S], [4Fe–4S], and [3Fe–4S]. FDX contains a [2Fe–2S] cluster [53]. SDHB contains three [Fe-S] clusters—[2Fe–2S], [4Fe–4S], and [3Fe–4S]—and was down-regulated by rifampicin and isoniazid combination treatment in *hPXR* mice in our analysis [54]. AOX1 and XDH (Supplementary Table S7) are [2Fe–2S]-containing proteins that were also down-regulated by isoniazid treatment in our analysis [55,56]. FECH contains a [2Fe–2S] cluster [57]. NDUFS8 was decreased and contains two [4Fe–4S] clusters, but the decrease was not mediated by isoniazid [58]. The effect of isoniazid on [Fe–S] clusters may be specific to [2Fe–2S] clusters.

### 3.2.5. [Fe–S] Cluster Assembly Machinery

The effects of isoniazid on heme biosynthesis, iron metabolism, and [Fe–S] cluster-containing proteins may also be associated with an effect on [Fe–S] cluster assembly machinery. Cysteine desulfurase (NFS1) significantly decreased ($p < 0.05$) in *hPXR* mice treated with the rifampicin and isoniazid

combination (0.89-relative change) or rifampicin alone (0.84-relative change). NFS1 also decreased to a lesser degree in *mPxr*$^{-/-}$ mice treated with both rifampicin and isoniazid (0.90 relative change). However, NFS1 changed less than 4% in *hPXR* mice treated with isoniazid (Supplementary Table S8). FDX1 significantly decreased ($p = 0.0016$) in all treatment groups and decreased to a greater degree with isoniazid alone (0.77-relative change) than with rifampicin alone (0.84-relative change). However, FDX1 decreased the most with the combination of rifampicin and isoniazid in *hPXR* mice (0.64-relative change). FDX1 also decreased in *mPxr*$^{-/-}$ mice treated with both rifampicin and isoniazid (0.79-relative change). The iron–sulfur cluster assembly 1 homolog (ISCA1) significantly decreased ($p = 0.0037$) from 0.66- to a 0.81-relative change in all treatment groups. BolA-like protein 3 (BOLA3) significantly decreased ($p = 0.012$) in *hPXR* mice treated with isoniazid (0.91-relative change) or the combination of rifampicin and isoniazid (0.89-relative change). However, BOLA3 increased in *hPXR* mice treated with rifampicin alone (1.12-relative change). The greatest effect of antitubercular therapy on [Fe–S] cluster assembly machinery in our analysis was on FDX1, which reduces CYPs and serves as an iron donor in the early steps of [Fe–S] cluster assembly [53].

### 3.2.6. Vitamin B$_6$ Metabolism

Isoniazid treatment is associated with vitamin B$_6$-dependent peripheral neuropathy, pellagra, and sideroblastic anemia [8,14,15,20]. A recent study demonstrated that isoniazid and vitamin B$_6$ conjugate to form pyridoxal isonicotinoyl hydrazone (PIH) [27]. If enough vitamin B$_6$ is depleted by conjugation with isoniazid, clinical vitamin B$_6$ deficiency may occur. This study also found that pyridoxal 5′-phosphate formed more PIH when combined with isoniazid than did nonphosphorylated forms of vitamin B$_6$ [27]. The vitamin B$_6$ metabolism enzymes pyridoxal kinase (PDXK) and pyridoxal-dependent decarboxylase domain-containing protein 1 (PDXDC1) did not significantly change in *hPXR* mice (Supplementary Table S9). Pyridoxal phosphate phosphatase (PDXP) significantly increased ($p = 0.00049$) at a 1.49-relative change in *hPXR* mice treated with both rifampicin and isoniazid, a 2.18-relative change in *hPXR* mice treated with rifampicin alone, and a 1.34-relative change in *mPxr*$^{-/-}$ mice treated with the rifampicin and isoniazid combination. PDXP significantly increased with rifampicin treatment alone and with the rifampicin and isoniazid combination in *hPXR* mice and in *mPxr*$^{-/-}$ mice (Supplementary Table S9). PDXP dephosphorylates pyridoxal 5′ phosphate to 4-pyridoxic acid but also dephosphorylates pyridoxine 5′ phosphate and pyridoxamine 5′ phosphate [59]. An increased dephosphorylation of vitamin B$_6$ by upregulated PDXP in response to rifampicin may increase the amount of PIH formed and subsequently decrease vitamin B$_6$ levels.

### 3.2.7. Homocysteine Metabolism

Antitubercular therapy is associated with homocysteinemia [12,60,61]. Proteins involved in homocysteine metabolism were affected by antitubercular therapy in our analysis (Supplementary Table S10). Methionine synthase significantly increased ($p < 0.05$) at a 1.26-relative change in *hPXR* mice treated with rifampicin. Betaine homocysteine S-methyltransferase 1 significantly increased ($p < 0.05$) in all treatment groups. Cystathionine β-synthase (CBS) significantly decreased ($p < 0.01$) in all treatment groups, but *hPXR* mice treated with both rifampicin and isoniazid or rifampicin alone (0.62-relative change) exhibited the largest decrease. Cystathionine γ-lyase significantly decreased ($p < 0.01$) at a 0.87-relative change in *hPXR* mice treated with rifampicin alone. Lower levels of CBS may result from increased serum homocysteine [62,63].

### 3.2.8. Tryptophan Metabolism

Proteins involved in tryptophan and vitamin B$_3$ metabolism were affected by antitubercular therapy in our analysis (Supplementary Table S11). The disruption of tryptophan metabolism can result in niacin deficiency. The 3-hydroxyanthranilate 3,4-dioxygenase (HAAO) significantly decreased ($p < 0.01$) in *hPXR* mice treated with rifampicin alone (0.91-relative change) or with the combination of rifampicin and isoniazid (0.91-relative change) but increased in *mPxr*$^{-/-}$ mice

(1.14-relative change). The kynurenine/alpha-aminoadipate aminotransferase (AADAT) significantly decreased ($p < 0.01$) in all treatment groups, with the greatest decrease occurring in *hPXR* mice treated with rifampicin alone (0.56-relative change). Kynurenine 3-monooxygenase (KMO) significantly decreased ($p < 0.05$) in *hPXR* mice treated with rifampicin alone (0.78-relative change) or with the combination of rifampicin and isoniazid (0.82-relative change), although isoniazid modestly decreased (0.91-relative change) KMO. In contrast, KMO increased (a 1.11-relative change) in $mPxr^{-/-}$ mice. Nicotinate phosphoribosyltransferase (NAPRT) significantly decreased ($p < 0.01$) in *hPXR* mice treated with rifampicin alone (0.83-relative change) or the combination of rifampicin and isoniazid (0.87-relative change) and in $mPxr^{-/-}$ mice treated with both rifampicin and isoniazid (0.79-relative change). The HAAO, AADAT, KMO, and NAPRT all decreased with rifampicin treatment alone. Specifically, HAAO and KMO decreased with rifampicin treatment in *hPXR* mice but not in $mPxr^{-/-}$ mice. Therefore, the effect of rifampicin on these proteins may be *hPXR* dependent. AADAT and KMO decreased with isoniazid treatment, but the magnitude of the decrease was higher with rifampicin treatment. These changes may result in systemic niacin depletion.

## 4. Discussion

We observed markedly elevated ALP and direct bilirubin levels, with histopathologic findings of bile plugs, in hPXR mice. These findings suggest a cholestatic pattern of DILI in response to rifampicin and isoniazid treatment, which recapitulates a previously reported milder phenotype of *hPXR*-dependent rifampicin- and isoniazid-induced DILI in mice [39,64–66]. Analysis of the liver proteome during the early stages of DILI may diminish the confounding effects of advanced hepatopathology in the later stages of DILI on the liver proteome. The control *hPXR* mice we used in our proteomic analysis had lower levels of hepatotoxicity than did *hPXR* mice treated with rifampicin and isoniazid, which had higher histopathologic scores. Correspondingly, the wound-healing proteins ANXA5, COL4A1, and TGM2 were increased in *hPXR* mice treated with both rifampicin and isoniazid. Therefore, our findings highlight the toxicoproteomic changes seen in *hPXR*-mediated antitubercular DILI without obfuscation by extensive tissue death.

Our profiling analysis revealed many changes in the proteins involved in relieving oxidative stress. Multiple GSTM isoforms were increased by rifampicin in an *hPXR*-dependent manner. GSTM-1 is reported to be protective in humans treated with rifampicin and isoniazid. Null alleles of *GSTM1* in humans may lead to increased DILI incidence [47,48,67–72]. In our study, rifampicin increased catalase in an *hPXR*-dependent manner, which may be protective by neutralizing $H_2O_2$. NQO1 is protective against acetaminophen (APAP)-induced hepatotoxicity and is increased in APAP-associated DILI [49] and primary biliary cirrhosis [73]. We found that NQO1 was increased in an *hPXR*-independent manner due to rifampicin and isoniazid combination treatment and to a greater extent from rifampicin treatment alone. Therefore, the rifampicin induction of *hPXR* may have imparted a protective effect on these oxidative stress proteins.

Cholestatic liver injury caused by rifampicin and isoniazid treatment was associated with PPIX accumulation and heme biosynthesis disruption, upregulated ALAS1, and downregulated FECH [27,39,40]. Furthermore, the effects on the heme biosynthetic pathway were due to the isoniazid metabolites hydrazine and PIH [27]. PIH is an iron chelator that forms from an enzyme-independent reaction between multiple vitamin $B_6$ orthologs and isoniazid. It also decreases FECH protein levels in an iron-dependent manner. Likewise, hydrazine increases ALAS1 at the mRNA and protein levels [27]. We and others have demonstrated ALAS1 up-regulation and FECH down-regulation in isoniazid-treated mice. Additional changes in the heme biosynthetic proteins BLVRA, PPOX, and UROS may also play a role in PPIX accumulation in an *hPXR*-independent manner. Rifampicin and isoniazid may induce PPIX formation to cause hepatotoxicity and exacerbated acute intermittent porphyria [5,6].

Isoniazid causes peripheral neuropathy secondary to vitamin $B_6$ depletion [14,16], with the conjugation of isoniazid to vitamin $B_6$ species (pyridoxal, pyridoxine, and pyridoxal 5′ phosphate) resulting in decreased vitamin $B_6$ levels in humans and rats and the formation of PIH [8,15,21,22,27].

Vitamin $B_6$ deficiency can lead to confusion, mood changes, seizures, stomatitis, cheilosis, and seborrheic dermatitis [74,75]. Rifampicin-mediated increased PDXP may lead to increased nonphosphorylated species of vitamin $B_6$, which form more PIH than phosphorylated species do [27,59]. We found this increase was most pronounced in *hPXR* mice treated with rifampicin alone. An increase of isoniazid-reactive forms of vitamin $B_6$ may contribute to the depletion of systemic vitamin $B_6$ stores. Therefore, rifampicin may disrupt vitamin $B_6$ metabolism in an hPXR-dependent manner, and isoniazid has been shown to disrupt vitamin $B_6$ metabolism in an hPXR-independent manner, previously [27].

Patients with tuberculosis are at an increased risk of deep vein thrombosis (DVT), pulmonary embolism (PE), and ischemic stroke [76–78], and antitubercular therapy may increase these risks, in addition to increased myocardial infarction risk [11–13,60]. Additionally, antitubercular therapy may cause homocysteinemia, which increases coagulability [12,60,61]. We found decreased cystathionine β-synthase in all treatment groups in an *hPXR*-independent manner. Cystathionine β-synthase is vitamin $B_6$-dependent and catalyzes the conversion of homocysteine to cystathionine. The decreased activity of this enzyme increases homocysteine levels [62,63]. We also found decreased cystathionine γ-lyase, which catalyzes the vitamin $B_6$-dependent conversion of cystathionine to cysteine, in *hPXR* mice treated with isoniazid in an *hPXR*-dependent manner. Decreases in these proteins may result in increased serum levels of homocysteine, which contribute to coagulopathy.

FTL1 was decreased in all treatment groups in an *hPXR*-independent manner, but the highest magnitude of decrease was in *hPXR* mice treated with both rifampicin and isoniazid. Low ferritin levels are a clinical sign of low systemic iron levels and may be caused by long-term exposure to an iron chelator. Deficiency of the iron transporter ABCB7 is associated with sideroblastic anemia, with ring sideroblasts from intracellular iron accumulation in erythrocytes [79]. ABCB7 exports [2Fe–2S] clusters out of the mitochondria and into the cytosol, and ABCB7 deficiency causes an iron-deficient phenotype and mitochondrial iron accumulation [79,80]. Indeed, sideroblastic anemia responsive to vitamin $B_6$ administration is reported with antitubercular therapy [8–10], and multiple types of anemia (including iron-deficiency anemia) occur with antitubercular therapy [81–83]. These data and previous reports suggest that isoniazid and rifampicin lead to an iron-deficient state, with concomitant changes in heme biosynthesis regulation.

A labile iron–sulfur [2Fe–2S] cluster is present in animal FECH but is absent in the analogous plant, bacterial, and yeast enzymes [84–86]. However, in mammals, when this structure is targeted by nitric oxide synthases, the degradation of FECH is increased [87–89]. The [2Fe–2S] cluster in FECH is most likely required for recycling rather than catalysis. Iron-limiting conditions decrease FECH protein levels by forming an unstable protein with a half-life of approximately 1 h, as compared with a half-life over 35 h in iron-replete conditions [90]. Therefore, an iron-limiting condition in the presence of PIH may lead to the formation of a FECH protein that is less stable than the protein formed in iron-replete conditions.

Iron-limiting conditions may also be associated with the down-regulation of other [Fe–S] cluster-containing proteins or [Fe–S] cluster assembly machinery proteins. The PIH-mediated FECH down-regulation of FECH is iron dependent [27]. The iron-limiting condition induced by deferoxamine reduces the half-life of FECH formed after treatment [90]. Indeed, we found two [Fe–S]-containing proteins down-regulated by isoniazid that contain multiple [Fe–S] clusters, some of which are [2Fe–2S] clusters. Multiple proteins containing [2Fe–2S] clusters were down-regulated by the rifampicin and isoniazid combination treatment independent of *hPXR*. This may be due to a reduced availability of iron to form [2Fe–2S] clusters or downstream effects during iron–sulfur cluster assembly. BOLA3, FDX1, ISCA1, and NFS1 were decreased by the rifampicin and isoniazid combination treatment in both *hPXR* and *mPxr*$^{-/-}$ mice. Whether these changes are direct effects of the drug treatment or are compensatory to other changes is unclear, but they do not appear to be caused by isoniazid treatment alone. The combination of rifampicin and isoniazid may decrease the ability to produce [Fe–S] clusters by affecting protein levels of cellular [Fe–S] cluster assembly machinery.

Hydrazine increases ALAS1 mRNA and protein [27] and is reported to N-alkylate, deactivate, and increase the turnover of CYP enzymes [91–94]. In addition to rifampicin-upregulated CYP enzymes, several CYP species were decreased by isoniazid in our analysis. Heme negatively regulates ALAS1 at the transcriptional, translational, and post-translational levels [95–99]. If hydrazine decreases the regulatory heme pool by the N-alkylation of cellular hematoproteins, this would result in ALAS1 up-regulation at both the protein and mRNA levels.

Rifampicin decreased the kynurenine pathway enzymes HAAO, AADAT, and KMO. The decreased HAAO and KMO may be mediated by *hPXR*. The kynurenine pathway catabolizes tryptophan to quinolinic acid for use in the nicotinamide adenine dinucleotide pathway. Deficiencies in this pathway disrupt tryptophan catabolism, and a nutritional deficiency in niacin or tryptophan causes vitamin $B_3$ (niacin) deficiency [100,101]. Antitubercular therapy can interfere with tryptophan metabolism, leading to decreased vitamin $B_3$ and pellagra, which is characterized by dermatitis, diarrhea, and dementia and can progress to death if untreated [18,19,102].

Our findings confirm and expand upon previous reports of antitubercular therapy disruption of the heme biosynthetic pathway [27,39,40]. Namely, antitubercular therapy affects proteins associated with [Fe–S] cluster assembly machinery, heme metabolism, homocysteine metabolism, iron metabolism, oxidative stress responses, tryptophan metabolism, vitamin $B_3$ metabolism, and vitamin $B_6$ metabolism. These findings may elucidate the pathophysiology of the antitubercular therapy complications of acute intermittent porphyria, anemia, DILI, drug–drug interactions, hypercoagulability (DVT, PE, ischemic strokes), pellagra, peripheral neuropathy, and porphyria cutanea tarda.

## 5. Conclusions

Isoniazid may play roles in such pathologic as hepatotoxicity, acute intermittent porphyria, anemia, pellagra (vitamin $B_3$ deficiency), vitamin $B_6$ deficiency, and hypercoagulable states (DVT, PE, or ischemic stroke). We observed hPXR-mediated changes in glutathione S-transferases, kynurenine pathway, vitamin B6 metabolism, and wound-healing proteins. We also observed hPXR-independent changes caused by rifampicin and isoniazid in [2Fe-2S] cluster-containing proteins, ABCB7, ferritin, and heme metabolism proteins. Our findings provide insight into the etiology of the mechanistic processes leading to these states after treatment with antitubercular therapy.

## References

1. Murray, C.J.L.; Ortblad, K.F.; Guinovart, C.; Lim, S.S.; Wolock, T.M.; Roberts, D.A.; Dansereau, E.A.; Graetz, N.; Barber, R.M.; Brown, J.C.; et al. Global, regional, and national incidence and mortality for HIV, tuberculosis, and malaria during 1990–2013: A systematic analysis for the Global Burden of Disease Study 2013. *Lancet* **2014**, *384*, 1005–1070. [CrossRef]

2. Singla, N.; Gupta, D.; Birbian, N.; Singh, J. Association of NAT2, GST and CYP2E1 polymorphisms and anti-tuberculosis drug-induced hepatotoxicity. *Tuberculosis* **2014**, *94*, 293–298. [CrossRef]

3. Tostmann, A.; Boeree, M.; Peters, W.H.; Roelofs, H.M.; Aarnoutse, R.; Van Der Ven, A.J.; Dekhuijzen, P.R. Isoniazid and its toxic metabolite hydrazine induce in vitro pyrazinamide toxicity. *Int. J. Antimicrob. Agents* **2008**, *31*, 577–580. [CrossRef] [PubMed]

4. Sharifzadeh, M.; Rasoulinejad, M.; Valipour, F.; Nouraie, M.; Vaziri, S. Evaluation of patient-related factors associated with causality, preventability, predictability and severity of hepatotoxicity during antituberculosis [correction of antituberclosis] treatment. *Pharmacol Res.* **2005**, *51*, 353–358. [CrossRef] [PubMed]

5. Golla, R.; Mukherjee, A.; Gone, R.K.; Singh, H.; Pannu, A.K.; Suri, V.; Bhalla, A. Acute Intermittent Porphyria & Anti-tuberculosis Therapy. *Qjm Int. J. Med.* **2019**. [CrossRef]

6. Treece, G.L.; Magnussen, C.R.; Patterson, J.R.; Tschudy, D.P. Exacerbation of porphyria during treatment of pulmonary tuberculosis. *Am. Rev. Respir. Dis.* **1976**, *113*, 233–237.

7. Kassa, E.; Enawgaw, B.; Gelaw, A.; Gelaw, B. Effect of anti-tuberculosis drugs on hematological profiles of tuberculosis patients attending at University of Gondar Hospital, Northwest Ethiopia. *Bmc Hematol.* **2016**, *16*, 1–11. [CrossRef] [PubMed]

8. Demiroglu, H.; Dündar, S. Vitamin B6 responsive sideroblastic anaemia in a patient with tuberculosis. *Br. J. Clin. Pr.* **1997**, *51*, 51–52.

9. Fratz-Berilla, E.J.; Breydo, L.; Gouya, L.; Puy, H.; Uversky, V.N.; Ferreira, G.C. Isoniazid inhibits human erythroid 5-aminolevulinate synthase: Molecular mechanism and tolerance study with four X-linked protoporphyria patients. *Biochim. Et Biophys. Acta (Bba) - Mol. Basis Dis.* **2017**, *1863*, 428–439. [CrossRef]

10. Piso, R.J.; Kriz, K.; Desax, M.-C. Severe isoniazid related sideroblastic anemia. *Hematol. Rep.* **2011**, *3*, 2. [CrossRef]

11. White, N. Venous thrombosis and rifampicin. *Lancet* **1989**, *334*, 434–435. [CrossRef]

12. Chaudhary, A.; Desai, U.; Joshi, J.M. Venous thromboembolism due to hyperhomocysteinaemia and tuberculosis. *Natl. Medj. India* **2017**, *30*, 139–141.

13. Sheu, J.-J.; Chiou, H.; Kang, J.-H.; Chen, Y.-H.; Lin, H.-C. Tuberculosis and the Risk of Ischemic Stroke: A 3-Year Follow-Up Study. *Stroke* **2010**, *41*, 244–249. [CrossRef] [PubMed]

14. Aita, J.F.; Calame, T.R. Peripheral neuropathy secondary to isoniazid-induced pyridoxine deficiency. *Md. State Medj.* **1972**, *21*, 68–70.

15. Carlson, H.B.; Anthony, E.M.; Russell, W.F.; Middlebrook, G. Prophylaxis of Isoniazid Neuropathy with Pyridoxine. *New Engl. J. Med.* **1956**, *255*, 118–122. [CrossRef]

16. Mahashur, A.A. Isoniazid induced peripheral neuropathy. *J. Assoc. Physicians India* **1992**, *40*, 651–652. [PubMed]

17. Millar, J.W. Rifampicin-induced porphyria cutanea tarda. *Br. J. Dis. Chest* **1980**, *74*, 405–408. [CrossRef]

18. Kipsang, J.K.; Choge, J.K.; Marinda, P.; Khayeka-Wandabwa, C. Pellagra in isoniazid preventive and antiretroviral therapy. *IDCases* **2019**, *17*, e00550. [CrossRef]

19. Bilgili, S.G.; Bilgili, S.G.; Calka, O.; Altun, F. Isoniazid-induced pellagra. *Cutan. Ocul. Toxicol.* **2011**, *30*, 317–319. [CrossRef]

20. Ishii, N.; Nishihara, Y. Pellagra encephalopathy among tuberculous patients: Its relation to isoniazid therapy. *J. Neurol. Neurosurg. Psychiatry* **1985**, *48*, 628–634. [CrossRef]

21. Sevigny, S.J.D.J.; White, S.L.; Halsey, M.L.; Johnston, F.A. Effect of Isoniazid on the Loss of Pyridoxal Phosphate from, and its Distribution in, the Body of the Rat. *J. Nutr.* **1966**, *88*, 45–50. [CrossRef] [PubMed]

22. Cilliers, K.; Labadarios, D.; Schaaf, H.S.; Willemse, M.; Maritz, J.; Werely, C.; Hussey, G.; Donald, P.R. Pyridoxal-5-phosphate plasma concentrations in children receiving tuberculosis chemotherapy including isoniazid. *Acta Paediatr.* **2010**, *99*, 705–710. [CrossRef] [PubMed]

23. Wang, Y.-M.; Chai, S.C.; Brewer, C.T.; Chen, T. Pregnane X receptor and drug-induced liver injury. *Expert Opin. Drug Metab. Toxicol.* **2014**, *10*, 1521–1532. [CrossRef] [PubMed]

24. Brewer, C.T.; Chen, T. PXR variants: The impact on drug metabolism and therapeutic responses. *Acta Pharm. Sin. B* **2016**, *6*, 441–449. [CrossRef] [PubMed]

25. Brewer, C.; Chen, T. Hepatotoxicity of Herbal Supplements Mediated by Modulation of Cytochrome P450. *Int. J. Mol. Sci.* **2017**, *18*, 2353. [CrossRef] [PubMed]

26. Brewer, C.T.; Low, J.; Chen, T. High-Throughput Imaging of PPIX Using Confocal Microscopy. *Breast Cancer* **2019**, *1966*, 137–149. [CrossRef]

27. Brewer, C.T.; Yang, L.; Edwards, A.; Lu, Y.; Low, J.; Wu, J.; Lee, R.E.; Chen, T. The Isoniazid Metabolites Hydrazine and Pyridoxal Isonicotinoyl Hydrazone Modulate Heme Biosynthesis. *Toxicol. Sci.* **2018**, *168*, 209–224. [CrossRef]

28. Xie, W.; Barwick, J.L.; Downes, M.; Blumberg, B.; Simon, C.M.; Nelson, M.C.; Neuschwander-Tetri, B.A.; Brunt, E.M.; Guzelian, P.S.; Evans, R.M. Humanized xenobiotic response in mice expressing nuclear receptor SXR. *Nature* **2000**, *406*, 435–439. [CrossRef]

29. Beaune, P.; Kremers, P.; Letawe-Goujon, F.; Gielen, J.E. Monoclonal antibodies against human liver cytochrome P-450. *Biochem. Pharmacol.* **1985**, *34*, 3547–3552. [CrossRef]

30. Schuetz, E.G.; Schinkel, A.H.; Relling, M.V.; Schuetz, J.D. P-glycoprotein: A major determinant of rifampicin-inducible expression of cytochrome P4503A in mice and humans. *Proc. Natl. Acad. Sci. USA* **1996**, *93*, 4001–4005. [CrossRef]

31. Wang, Y.-M.; Lin, W.; Chai, S.C.; Wu, J.; Ong, S.S.; Schuetz, E.G.; Chen, T. Piperine activates human pregnane X receptor to induce the expression of cytochrome P450 3A4 and multidrug resistance protein 1. *Toxicol. Appl. Pharmacol.* **2013**, *272*, 96–107. [CrossRef] [PubMed]

32. Pagala, V.R.; High, A.A.; Wang, X.; Tan, H.; Kodali, K.; Mishra, A.; Kavdia, K.; Xu, Y.; Wu, Z.; Peng, J. Quantitative Protein Analysis by Mass Spectrometry. *Adv. Struct. Saf. Stud.* **2015**, *1278*, 281–305. [CrossRef]

33. Lin, W.; Wang, Y.-M.; Chai, S.C.; Lv, L.; Zheng, J.; Wu, J.; Zhang, Q.; Wang, Y.-D.; Griffin, P.R.; Chen, T. SPA70 is a potent antagonist of human pregnane X receptor. *Nat. Commun.* **2017**, *8*, 741. [CrossRef] [PubMed]

34. Bai, B.; Tan, H.; Pagala, V.R.; High, A.A.; Ichhaporia, V.; Hendershot, L.; Peng, J. Deep Profiling of Proteome and Phosphoproteome by Isobaric Labeling, Extensive Liquid Chromatography and Mass Spectrometry. *Methods Enzymol.* **2016**, *585*, 377–395. [CrossRef]

35. Wang, X.; Li, Y.; Wu, Z.; Wang, H.; Tan, H.; Peng, J. JUMP: A tag-based database search tool for peptide identification with high sensitivity and accuracy. *Mol. Cell. Proteom.* **2014**, *13*, 3663–3673. [CrossRef]

36. Niu, M.; Cho, J.-H.; Kodali, K.; Pagala, V.; High, A.A.; Wang, H.; Wu, Z.; Li, Y.; Bi, W.; Zhang, H.; et al. Extensive Peptide Fractionation and y1 Ion-Based Interference Detection Method for Enabling Accurate Quantification by Isobaric Labeling and Mass Spectrometry. *Anal. Chem.* **2017**, *89*, 2956–2963. [CrossRef]

37. Bai, B.; Wang, X.; Li, Y.; Chen, P.-C.; Yu, K.; Dey, K.K.; Yarbro, J.M.; Han, X.; Lutz, B.M.; Rao, S.; et al. Deep Multilayer Brain Proteomics Identifies Molecular Networks in Alzheimer's Disease Progression. *Neuron* **2020**, *106*, 700. [CrossRef]

38. Perez-Riverol, Y.; Csordas, A.; Bai, J.; Bernal-Llinares, M.; Hewapathirana, S.; Kundu, D.J.; Inuganti, A.; Griss, J.; Mayer, G.; Eisenacher, M.; et al. The PRIDE database and related tools and resources in 2019: Improving support for quantification data. *Nucleic Acids Res.* **2018**, *47*, D442–D450. [CrossRef]

39. Li, F.; Lu, J.; Cheng, J.; Wang, L.; Matsubara, T.; Csanaky, I.L.; Klaassen, C.D.; Gonzalez, F.J.; Ma, X. Human PXR modulates hepatotoxicity associated with rifampicin and isoniazid co-therapy. *Nat. Med.* **2013**, *19*, 418–420. [CrossRef]

40. Sachar, M.; Li, F.; Liu, K.; Wang, P.; Lu, J.; Ma, X. Chronic Treatment with Isoniazid Causes Protoporphyrin IX Accumulation in Mouse Liver. *Chem. Res. Toxicol.* **2016**, *29*, 1293–1297. [CrossRef]

41. Muruganandan, S.; Sinal, C. Mice as Clinically Relevant Models for the Study of Cytochrome P450-dependent Metabolism. *Clin. Pharmacol. Ther.* **2008**, *83*, 818–828. [CrossRef] [PubMed]

42. Yamada, S.; Tang, M.; Richardson, K. Genetic variations of NAT2 and CYP2E1 and isoniazid hepatotoxicity in a diverse population. *Pharmacogenomics* **2009**, *10*, 1433–1445. [CrossRef] [PubMed]

43. Gogtay, N.; Kapileshwar, S.R.; Shah, S.U.; Bendkhale, S.R.; Ramakrishna, S.; Sridharan, K.; Thelma, B.K.; Thatte, U.M.; Kshirsagar, N.A. Evaluation of cytochrome P4502E1 polymorphisms in healthy adult Western Indians and patients with antituberculous drug-induced hepatotoxicity. *Indianj. Pharmacol.* **2016**, *48*, 42–46. [CrossRef] [PubMed]

44. Butov, D.; Antonenko, P.; Kresyun, V.; Antonenko, K.; Butova, T. Association between effectiveness of tuberculosis treatment and cytochrome P-4502E1 polymorphism of the patients. *Int. J. Mycobacteriology* **2017**, *6*, 396. [CrossRef]

45. Lian, Y.; Zhao, J.; Wang, Y.-M.; Zhao, J.; Peng, S.-Q. Metallothionein protects against isoniazid-induced liver injury through the inhibition of CYP2E1-dependent oxidative and nitrosative impairment in mice. *Food Chem. Toxicol.* **2017**, *102*, 32–38. [CrossRef]

46. Cheng, J.; Krausz, K.W.; Li, F.; Ma, X.; Gonzalez, F.J. CYP2E1-dependent elevation of serum cholesterol, triglycerides, and hepatic bile acids by isoniazid. *Toxicol. Appl. Pharmacol.* **2013**, *266*, 245–253. [CrossRef]

47. Gupta, V.H.; Singh, M.; Amarapurkar, D.N.; Sasi, P.; Joshi, J.M.; Baijal, R.; Kumar, H.R.P.; Amarapurkar, A.D.; Joshi, K.; Wangikar, P.P. Association of GST null genotypes with anti-tuberculosis drug induced hepatotoxicity in Western Indian population. *Ann. Hepatol.* **2013**, *12*, 959–965. [CrossRef]

48. Li, C.; Long, J.; Hu, X.; Zhou, Y. GSTM1 and GSTT1 genetic polymorphisms and risk of anti-tuberculosis drug-induced hepatotoxicity: An updated meta-analysis. *Eur. J. Clin. Microbiol. Infect. Dis.* **2013**, *32*, 859–868. [CrossRef]

49. Hwang, J.H.; Kim, Y.-H.; Noh, J.-R.; Gang, G.-T.; Kim, K.-S.; Chung, H.K.; Tadi, S.; Yim, Y.-H.; Shong, M.; Lee, C.-H. The protective role of NAD(P)H:quinone oxidoreductase 1 on acetaminophen-induced liver injury is associated with prevention of adenosine triphosphate depletion and improvement of mitochondrial dysfunction. *Arch. Toxicol.* **2014**, *89*, 2159–2166. [CrossRef]

50. Hashimoto, K.; Kim, H.; Oishi, H.; Chen, M.; Iskender, I.; Sakamoto, J.; Ohsumi, A.; Guan, Z.; Hwang, D.; Waddell, T.K.; et al. Annexin V homodimer protects against ischemia reperfusion–induced acute lung injury in lung transplantation. *J. Thorac. Cardiovasc. Surg.* **2016**, *151*, 861–869. [CrossRef]

51. Zakrzewicz, A.; Atanasova, S.; Padberg, W.; Grau, V. Monocytic Tissue Transglutaminase in a Rat Model for Reversible Acute Rejection and Chronic Renal Allograft Injury. *Mediat. Inflamm.* **2015**, *2015*, 1–13. [CrossRef]

52. Thankam, F.G.; Chandra, I.; Diaz, C.; Dilisio, M.F.; Fleegel, J.; Gross, R.M.; Agrawal, D.K. Matrix regeneration proteins in the hypoxia-triggered exosomes of shoulder tenocytes and adipose-derived mesenchymal stem cells. *Mol. Cell. Biochem.* **2019**, *465*, 75–87. [CrossRef] [PubMed]

53. Sheftel, A.D.; Stehling, O.; Pierik, A.J.; Elsässer, H.-P.; Mühlenhoff, U.; Webert, H.; Hobler, A.; Hannemann, F.; Bernhardt, R.; Lill, R. Humans possess two mitochondrial ferredoxins, Fdx1 and Fdx2, with distinct roles in steroidogenesis, heme, and Fe/S cluster biosynthesis. *Proc. Natl. Acad. Sci. USA* **2010**, *107*, 11775–11780. [CrossRef] [PubMed]

54. Sun, F.; Huo, X.; Zhai, Y.; Wang, A.; Xu, J.; Su, D.; Bartlam, M.; Rao, Z. Crystal Structure of Mitochondrial Respiratory Membrane Protein Complex II. *Cell* **2005**, *121*, 1043–1057. [CrossRef] [PubMed]

55. Coelho, C.; Foti, A.; Hartmann, T.; Santos-Silva, T.; Leimkühler, S.; Romao, M. Structural insights into xenobiotic and inhibitor binding to human aldehyde oxidase. *Nat. Methods* **2015**, *11*, 779–783. [CrossRef]

56. Nishino, T.; Okamoto, K. The role of the [2Fe–2S] cluster centers in xanthine oxidoreductase. *J. Inorg. Biochem.* **2000**, *82*, 43–49. [CrossRef]

57. Crouse, B.R.; Sellers, V.M.; Finnegan, M.G.; Dailey, H.A.; Johnson, M.K. Site-Directed Mutagenesis and Spectroscopic Characterization of Human Ferrochelatase: Identification of Residues Coordinating the [2Fe-2S] Cluster†. *Biochemistry* **1996**, *35*, 16222–16229. [CrossRef]

58. Loeffen, J.; Smeitink, J.; Triepels, R.; Smeets, R.; Schuelke, M.; Sengers, R.; Trijbels, F.; Hamel, B.; Mullaart, R.; Heuvel, L.V.D. The First Nuclear-Encoded Complex I Mutation in a Patient with Leigh Syndrome. *Am. J. Hum. Genet.* **1998**, *63*, 1598–1608. [CrossRef]

59. Jang, Y.M.; Kim, D.W.; Kang, T.-C.; Won, M.H.; Baek, N.-I.; Moon, B.J.; Choi, S.Y.; Kwon, O.-S. Human Pyridoxal Phosphatase. *J. Boil. Chem.* **2003**, *278*, 50040–50046. [CrossRef]

60. Ren, M.-Y.; Zhang, C.-S.; Zhang, X.-J.; Zhong, J.-Q. Acute Myocardial Infarction in a Young Man with Hyperhomocysteinemia and Pulmonary Tuberculosis. *Intern. Med.* **2016**, *55*, 153–159. [CrossRef]

61. Wald, D.S.; Law, M.; Morris, J.K. Homocysteine and cardiovascular disease: Evidence on causality from a meta-analysis. *BMJ* **2002**, *325*, 1202. [CrossRef] [PubMed]

62. Watanabè, M.; Osada, J.; Aratani, Y.; Kluckman, K.; Reddick, R.; Malinow, M.R.; Maeda, N. Mice deficient in cystathionine beta-synthase: Animal models for mild and severe homocyst(e)inemia. *Proc. Natl. Acad. Sci. USA* **1995**, *92*, 1585–1589. [CrossRef] [PubMed]

63. Smolin, L.A.; Benevenga, N.J. Accumulation of homocyst(e)ine in vitamin B-6 deficiency: A model for the study of cystathionine beta-synthase deficiency. *J. Nutr.* **1982**, *112*, 1264–1272. [CrossRef] [PubMed]

64. Chen, X.; Xu, J.; Zhang, C.; Yu, T.; Wang, H.; Zhao, M.; Duan, Z.-H.; Zhang, Y.; Xu, J.-M.; Xu, D.-X. The protective effects of ursodeoxycholic acid on isoniazid plus rifampicin induced liver injury in mice. *Eur. J. Pharmacol.* **2011**, *659*, 53–60. [CrossRef] [PubMed]

65. Guo, H.-L.; Hassan, H.M.; Ding, P.-P.; Wang, S.; Chen, X.; Wang, T.; Sun, L.-X.; Zhang, L.; Jiang, Z. Pyrazinamide-induced hepatotoxicity is alleviated by 4-PBA via inhibition of the PERK-eIF2$\alpha$-ATF4-CHOP pathway. *Toxicology* **2017**, *378*, 65–75. [CrossRef]

66. Kim, J.-H.; Nam, W.S.; Kim, S.J.; Kwon, O.K.; Seung, E.J.; Jo, J.J.; Shresha, R.; Lee, T.H.; Jeon, T.W.; Ki, S.H.; et al. Mechanism Investigation of Rifampicin-Induced Liver Injury Using Comparative Toxicoproteomics in Mice. *Int. J. Mol. Sci.* **2017**, *18*, 1417. [CrossRef]

67. Roy, B.; Chowdhury, A.; Kundu, S.; Santra, A.; Dey, B.; Chakraborty, M.; Majumder, P.P. Increased risk of antituberculosis drug-induced hepatotoxicity in individuals with glutathione S-transferase M1 'null' mutation. *J. Gastroenterol. Hepatol.* **2001**, *16*, 1033–1037. [CrossRef]

68. Huang, Y.-S.; Su, W.-J.; Huang, Y.-H.; Chen, C.-Y.; Chang, F.-Y.; Lin, H.; Lee, S.-D. Genetic polymorphisms of manganese superoxide dismutase, NAD(P)H:quinone oxidoreductase, glutathione S-transferase M1 and T1, and the susceptibility to drug-induced liver injury. *J. Hepatol.* **2007**, *47*, 128–134. [CrossRef]

69. Lucena, M.I.; Andrade, R.J.; Martínez, C.; Ulzurrun, E.; Garcia-Martin, E.; Borraz, Y.; Fernandez, M.C.; Romero-Gomez, M.; Castiella, A.; Planas, R.; et al. GlutathioneS-transferase m1 and t1 null genotypes increase susceptibility to idiosyncratic drug-induced liver injury. *Hepatology* **2008**, *48*, 588–596. [CrossRef]

70. Bing, C.; Xiaomeia, C.; Jinhenga, L. Gene dose effect of NAT2 variants on the pharmacokinetics of isoniazid and acetylisoniazid in healthy Chinese subjects. *Drug Metab. Drug Interact.* **2011**, *26*, 113–118. [CrossRef]

71. Monteiro, T.P.; El-Jaick, K.; Jeovanio-Silva, A.L.; Brasil, P.E.A.A.D.; Costa, M.J.M.; Rolla, V.C.; De Castro, L. The roles of GSTM1 and GSTT1 null genotypes and other predictors in anti-tuberculosis drug-induced liver injury. *J. Clin. Pharm. Ther.* **2012**, *37*, 712–718. [CrossRef]

72. Tang, N.; Deng, R.; Wang, Y.; Lin, M.; Li, H.; Qiu, Y.; Hong, M.; Zhou, G. GSTM1 and GSTT1 null polymorphisms and susceptibility to anti-tuberculosis drug-induced liver injury: A meta-analysis [Review article]. *Int. J. Tuberc. Lung Dis.* **2013**, *17*, 17–25. [CrossRef] [PubMed]

73. Aleksunes, L.M.; Klaassen, C.D. Coordinated regulation of hepatic phase I and II drug-metabolizing genes and transporters using AhR-, CAR-, PXR-, PPAR$\alpha$-, and Nrf2-null mice. *Drug Metab. Dispos.* **2012**, *40*, 1366–1379. [CrossRef]

74. Scriver, C.R.; Hutchison, J.H. The vitamin B6 deficiency syndrome in human infancy: Biochemical and clinical observations. *Pediatrics* **1963**, *31*, 240–250.

75. Vilter, R.W.; Mueller, J.F.; Glazer, H.S.; Jarrold, T.; Abraham, J.; Thompson, C.; Hawkins, V.R. The effect of vitamin B6 deficiency induced by desoxypyridoxine in human beings. *J. Lab. Clin. Med.* **1953**, *42*, 335–357. [PubMed]

76. Ha, H.; Kim, K.H.; Park, J.H.; Lee, J.-K.; Heo, E.Y.; Kim, J.-S.; Kim, D.-K.; Choi, I.S.; Chung, H.S.; Lim, H.J. Thromboembolism in Mycobacterium tuberculosis Infection: Analysis and Literature Review. *Infect. Chemother.* **2019**, *51*, 142–149. [CrossRef]

77. Cowie, R.; Dansey, R.; Hay, M. Deep-vein thrombosis and pulmonary tuberculosis. *Lancet* **1989**, *334*, 1397. [CrossRef]

78. Kechaou, I.; Cherif, E.; Ben Hassine, L.; Khalfallah, N. Deep vein thrombosis and tuberculosis: A causative link? *Bmj Case Rep.* **2014**, *2014*. [CrossRef]

79. Pondarre, C.; Campagna, D.R.; Antiochos, B.; Sikorski, L.; Mulhern, H.; Fleming, M.D. Abcb7, the gene responsible for X-linked sideroblastic anemia with ataxia, is essential for hematopoiesis. *Blood* **2006**, *109*, 3567–3569. [CrossRef]

80. Cavadini, P.; Biasiotto, G.; Poli, M.; Levi, S.; Verardi, R.; Zanella, I.; Derosas, M.; Ingrassia, R.; Corrado, M.; Arosio, P. RNA silencing of the mitochondrial ABCB7 transporter in HeLa cells causes an iron-deficient phenotype with mitochondrial iron overload. *Blood* **2006**, *109*, 3552–3559. [CrossRef] [PubMed]

81. Lee, S.W.; Kang, Y.A.; Yoon, Y.S.; Um, S.-W.; Lee, S.M.; Yoo, C.-G.; Kim, Y.W.; Han, S.K.; Shim, Y.-S.; Yim, J.-J. The Prevalence and Evolution of Anemia Associated with Tuberculosis. *J. Korean Med. Sci.* **2006**, *21*, 1028–1032. [CrossRef] [PubMed]

82. Baynes, R.D.; Flax, H.; Bothwell, T.H.; Bezwoda, W.R.; MacPhail, A.P.; Atkinson, P.; Lewis, D. Haematological and iron-related measurements in active pulmonary tuberculosis. *Scand. J. Haematol.* **1986**, *36*, 280–287. [CrossRef] [PubMed]

83. Kaeley, N.; Mukherjee, A.; Dhar, M.; Kumar, S.; Bhushan, B. Prevalence, characteristics, and predictors of tuberculosis associated anemia. *J. Fam. Med. Prim. Care* **2019**, *8*, 2445–2449. [CrossRef] [PubMed]

84. Dailey, H.A.; Finnegan, M.G.; Johnson, M.K. Human ferrochelatase is an iron-sulfur protein. *Biochemistry* **1994**, *33*, 403–407. [CrossRef]

85. Ferreira, G.C.; Gong, J. 5-Aminolevulinate synthase and the first step of heme biosynthesis. *J. Bioenerg. Biomembr.* **1995**, *27*, 151–159. [CrossRef]

86. Day, A.L.; Parsons, B.M.; Dailey, H.A. Cloning and Characterization ofGallusandXenopusFerrochelatases: Presence of the [2Fe-2S] Cluster in Nonmammalian Ferrochelatase. *Arch. Biochem. Biophys.* **1998**, *359*, 160–169. [CrossRef]

87. Sellers, V.M.; Johnson, M.K.; Dailey, H.A. Function of the [2Fe−2S] Cluster in Mammalian Ferrochelatase: A Possible Role as a Nitric Oxide Sensor†. *Biochemistry* **1996**, *35*, 2699–2704. [CrossRef]

88. Kim, Y.-M.; Bergonia, H.A.; Müller, C.; Pitt, B.R.; Watkins, W.D.; Lancaster, J.R. Loss and Degradation of Enzyme-bound Heme Induced by Cellular Nitric Oxide Synthesis. *J. Boil. Chem.* **1995**, *270*, 5710–5713. [CrossRef]

89. Rouault, T.A.; Klausner, R.D. Iron-sulfur clusters as biosensors of oxidants and iron. *Trends Biochem. Sci.* **1996**, *21*, 174–177. [CrossRef]

90. Crooks, D.R.; Ghosh, M.C.; Haller, R.G.; Tong, W.-H.; Rouault, T.A. Posttranslational stability of the heme biosynthetic enzyme ferrochelatase is dependent on iron availability and intact iron-sulfur cluster assembly machinery. *Blood* **2010**, *115*, 860–869. [CrossRef]

91. Battioni, P.; Mahy, J.-P.; Delaforge, M.; Mansuy, D. Reaction of Monosubstituted Hydrazines and Diazenes with Rat-Liver Cytochrome P450. Formation of Ferrous-Diazene and Ferric sigma-Alkyl Complexes. *Jbic J. Boil. Inorg. Chem.* **1983**, *134*, 241–248. [CrossRef] [PubMed]

92. Ator, M.A.; David, S.K.; De Montellano, P.R.O. Structure and catalytic mechanism of horseradish peroxidase. Regiospecific meso alkylation of the prosthetic heme group by alkylhydrazines. *J. Boil. Chem.* **1987**, *262*, 14954–14960.

93. Jenner, A.M.; Timbrell, J.A. Effect of acute and repeated exposure to low doses of hydrazine on hepatic microsomal enzymes and biochemical parameters in vivo. *Arch. Toxicol.* **1994**, *68*, 240–245. [CrossRef] [PubMed]

94. Wen, X.; Wang, J.-S.; Neuvonen, P.J.; Backman, J.T. Isoniazid is a mechanism-based inhibitor of cytochrome P450 1A2, 2A6, 2C19 and 3A4 isoforms in human liver microsomes. *Eur. J. Clin. Pharmacol.* **2002**, *57*, 799–804. [CrossRef] [PubMed]

95. Kolluri, S.; Sadlon, T.J.; May, B.K.; Bonkovsky, H.L. Haem repression of the housekeeping 5-aminolaevulinic acid synthase gene in the hepatoma cell line LMH. *Biochem. J.* **2005**, *392*, 173–180. [CrossRef]

96. Yoshino, K.; Munakata, H.; Kuge, O.; Ito, A.; Ogishima, T. Haeme-regulated Degradation of -Aminolevulinate Synthase 1 in Rat Liver Mitochondria. *J. Biochem.* **2007**, *142*, 453–458. [CrossRef]

97. Zheng, J.; Shan, Y.; Lambrecht, R.W.; Donohue, S.E.; Bonkovsky, H.L. Differential regulation of human ALAS1 mRNA and protein levels by heme and cobalt protoporphyrin. *Mol. Cell. Biochem.* **2008**, *319*, 153–161. [CrossRef]

98. Gotoh, S.; Nakamura, T.; Kataoka, T.; Taketani, S. Egr-1 regulates the transcriptional repression of mouse delta-aminolevulinic acid synthase 1 by heme. *Gene* **2011**, *472*, 28–36. [CrossRef]

99. Kubota, Y.; Nomura, K.; Katoh, Y.; Yamashita, R.; Kaneko, K.; Furuyama, K. Novel Mechanisms for Heme-dependent Degradation of ALAS1 Protein as a Component of Negative Feedback Regulation of Heme Biosynthesis*. *J. Boil. Chem.* **2016**, *291*, 20516–20529. [CrossRef]

100. Schwarcz, R.; Stone, T.W. The kynurenine pathway and the brain: Challenges, controversies and promises. *Neuropharmacol.* **2017**, *112*, 237–247. [CrossRef]

101. Goldsmith, G.A.; Sarett, H.P.; Register, U.D.; Gibbens, J. Studies of niacin requirement in man. i. experimental pellagra in subjects on corn diets low in niacin and tryptophan 1. *J. Clin. Investig.* **1952**, *31*, 533–542. [CrossRef] [PubMed]

102. Griffiths, W.A.D.; Greaves, M.W.; Meara, R.H. Isoniazid-Induced Pellagra. *Proc. R. Soc. Med.* **1976**, *69*, 313–314. [CrossRef] [PubMed]